ELSEVIER

Contents lists available at ScienceDirect

# Physics of the Earth and Planetary Interiors

journal homepage: www.elsevier.com/locate/pepi





# Effects of pressure on diffusion creep in wet olivine aggregates

Reynold E. Silber\*, Jennifer Girard, Shun-ichiro Karato

Department of Earth and Planetary Science, Yale University, New Haven 06511, CT, USA

ABSTRACT

We report the results of an experimental study to determine the influence of pressure on diffusion creep in wet olivine. In order to observe diffusion creep at high-pressure conditions at laboratory strain rates, we prepared ultra-fine grained (0.22–0.72 µm) olivine aggregates both from San Carlos olivine and from oxide mixtures using a solgel technique. All samples contain some water (~1000 ppm wt) presumably due to adsorption on fine-grained powder samples. We used Deformation-DIA (D-DIA) coupled with synchrotron X-ray facility (6-BM-B beamline at APS) to perform in-situ high pressure (3–10 GPa) deformation experiments in the temperature range 973–1123 K. The operation of diffusion creep in our samples was inferred from the weak (hkl) dependence of lattice strain, the much smaller strength of our samples compared to the strength expected for dislocation creep, and the estimate of stress exponent. Diffusion creep was also confirmed from a comparison to previous results on diffusion creep at lower pressures. We assume the flow low of the following form  $\dot{\epsilon} \propto C_W^r d^{-m} exp \left( -\frac{pV}{RT} \right)$  ( $\dot{\epsilon}$ : strain rate,  $C_W$ : water content, d: grain size) with r=0.7–1.0 and m=2 or 3, from which we obtain the activation volume ( $V^*$ ) of 2.5 +/- 0.6 cm<sup>3</sup>/mol. This activation volume is substantially smaller than that for dislocation creep implying that diffusion creep plays an important role in the deep upper mantle. Some implications for seismic anisotropy are also discussed.

### 1. Introduction

Plastic properties of the upper mantle materials have an important influence on the dynamics of this region including the depth and regional variation of mantle flow and the distribution of seismic anisotropy. A volumetrically large fraction (~50-70%) of the upper mantle is made of olivine (e.g., Ringwood, 1975), and olivine is softer than other minerals at least under high temperature conditions (e.g., Farla et al., 2013). Consequently, plastic properties of olivine have been investigated during the last ~50 years (e.g., Darot and Gueguen, 1981; Karato and Jung, 2003; Karato et al., 1986; Kohlstedt and Goetze, 1974; Mei and Kohlstedt, 2000a, 2000b; Chen et al., 1998). Among them, using synthetic fine-grained olivine aggregates, Karato et al. (1986) identified both dislocation and diffusion creep and found that deformation by both mechanisms is enhanced by water. By extrapolating their data to coarse grain size and higher pressures, they suggested a possible transition between dislocation and diffusion creep in Earth's upper mantle (Karato, 1992; Karato and Wu, 1993).

These studies suggest a depth variation in the dominant mechanism of deformation, but one of the key parameters such as activation volume  $V^*$  (the pressure dependence of creep strength) for diffusion creep was not determined experimentally. Only one experimental study (Mei and Kohlstedt, 2000a) measured  $V^*$  for diffusion creep in olivine and reported an activation volume of  $15 \pm 5 \, \mathrm{cm}^3/\mathrm{mol}$ . However, these results are subject to a large uncertainty since the pressure range is small (0.10

< P < 0.45 GPa). The absence of high-pressure experimental data and large uncertainties in activation volume cause large uncertainties in our understanding of rheological properties of the upper mantle (Hirth and Kohlstedt, 2003; Karato and Wu, 1993).

In the meantime, new techniques were developed to conduct quantitative deformation experiments under high pressures using synchrotron facilities (Karato and Weidner, 2008; Weidner, 2018; Wang et al., 2003). Those techniques allow us to conduct deformation experiment on olivine under the conditions of the entire upper mantle pressure (P) to  $\sim$ 13 GPa, temperature (T) to  $\sim$ 1800 K (e.g., Durham et al., 2009; Kawazoe et al., 2009; Li et al., 2006). However, all these previous studies were on dislocation creep and there was no study on diffusion creep under deep upper mantle conditions.

The reason for this is that, at such high pressures, minerals become so strong and hence the stress needed for deformation under the laboratory strain rate is high and consequently dislocation creep dominates over diffusion creep if we use the grain size of  $\sim\!10~\mu m$ , which is a typical grain size used in most of deformation experiments (e.g., Karato et al., 1986; Mei and Kohlstedt, 2000a). Recently, Nishihara et al. (2014) reported experimental results on deformation of fine-grained ( $\sim\!1~\mu m$ ) relatively dry olivine at higher pressures (P=3.0 to 5.3 GPa) and determined the flow law parameters such the stress exponent and the activation volume. However, their experimental conditions are inbetween two (or more) different deformation mechanisms (the overall stress exponent is n=1.9 and overall activation volume is 11.2 cm³/

E-mail address: reynold.silber@gmail.com (R.E. Silber).

<sup>\*</sup> Corresponding author.

mol), and therefore, flow law parameters in the individual mechanism are not well constrained. These previous observations suggest that in order to determine the flow law of diffusion creep under high pressure conditions, one needs to prepare samples with grain size smaller than 1  $\mu m$  at slow strain rate and relatively low temperatures. In fact, Mohiuddin et al. (2020) observed diffusion creep in ringwoodite only for samples with very small grain size (0.015–0.020  $\mu m$ ) and at  $T\sim 1173$  K. Therefore, to investigate the effects of pressure on diffusion creep, we prepared ultrafine-grained ( $\sim\!0.22{-}0.72~\mu m$ ) olivine polycrystals and deformed them at a pressure range of 3 to 10 GPa. We also chose relatively low temperatures ( $\sim\!973{-}1123$  K) to minimize grain-growth and to increase the relative importance of diffusion creep over dislocation creep. The samples used include those made from San Carlos olivine as well as the ones based on solution-gelation-derived olivine (solgel) synthesis technique.

### 2. Methods

### 2.1. Sample preparation

San Carlos olivine  $(Mg_{0.91},Fe_{0.09})_2SiO_4$ , and solgel samples were prepared separately. Preparation of San Carlos (SC) olivine samples was done following the procedure described by Karato et al. (1986). First, clean San Carlos olivine crystals were handpicked and crushed and then subsequently ground in a ball mill for at least 24 h. The sedimentation technique was used to separate the powder with grain sizes in the range of 100-200 nm. Subsequently, the powder was mixed with 1 wt% orthopyroxene (opx) and up to 5 wt% nano-size (0.013  $\mu$ m) alumina to control the silicate activity and mitigate the grain growth. The mixed powder was then baked at 1273 K in a controlled oxygen fugacity gas furnace before it was densely packed into the Ni capsule (to control oxygen fugacity) and hot pressed at 3 GPa and 1073 K for one hour.

Solgel samples were synthesized following the technique used by Faul and Jackson (2007). Magnesium and iron nitrates were dissolved in ethanol and mixed with tetraethyl orthosilicate. The mixture was heated on a hot plate at 30 °C and gelation was initiated by adding small amount of nitric acid (HNO3) and continually stirred with a magnetic stirrer until the mixture was completely dry. The collected solution was subsequently dried completely at 1273 K under well controlled oxygen fugacity using CO2 and H2 gas mixture ( $f_{\rm O2} \sim 10^{-8}$ – $10^{-9}$  atm) to synthesize olivine with composition (Fe<sub>0.1</sub>,Mg<sub>0.9</sub>)<sub>2</sub>SiO<sub>4</sub>. 1 wt% orthopyroxene was added to the solgel and mixed with again 5 wt% nano alumina to control the silica activity and mitigate the grain growth, respectively. To remove the porosity, the synthesized crystalline material was ground again and hot pressed in the same way as San Carlos olivine.

# 2.2. Grain size and water content measurements

Hot-pressed samples were removed from the Ni capsule, core drilled into cylinders of 1.3 mm long and 1 mm diameter. The representative samples from each hot-pressing run were prepared and subsequently probed using a Scanning Electron Microscope (SEM) (FEI/Philips XL30 ESEM-FEG) to determine the grain size using the intercept method and using the conversion factor of 1.5. Not only the average grain size, but also the grain size distribution was determined. To convert the measured distribution of intercept length to the distribution of grain size, the method of Cahn and Fullman (1956) as well as Abrams (1971) was used. The average grain size for solgel olivine was determined to be in the range of  ${\sim}0.22~\mu m$ . For two hot-pressed San Carlos olivine sample batches, the grain sizes were measured to be  ${\sim}0.30$  and  ${\sim}~0.72~\mu m,$ respectively. We note that due to extremely small grain sizes, the grain boundaries could not be resolved reliably using SEM on acid etched surfaces. Consequently, SEM probe and subsequent grain size analysis were performed on fractured sample surfaces. The representative SEM photomicrographs for San Carlos and solgel olivine are shown in Fig. S1.

**Table 1**Characterization results of samples synthesized in a Kawai apparatus (grain size and water content results). For grain size uncertainties, the errors are given as half widths of the semi-logarithmic 'Gaussian' plot of grain sizes in Fig. 5.

	San Carlos Oliv	ine	Solgel			
Kawai Run # Grain size (µm) Water COH	K1984 0.30 ± (0.16, 0.20)	K1982 0.72 ± (0.43, 0.54)	K1976 $0.25 \pm (0.11, 0.15)$	K1981 $0.22 \pm (0.10, 0.13)$		
(ppm wt)	$1075\pm107$	$1075\pm107$	$1010\pm100$	$1010\pm100$		

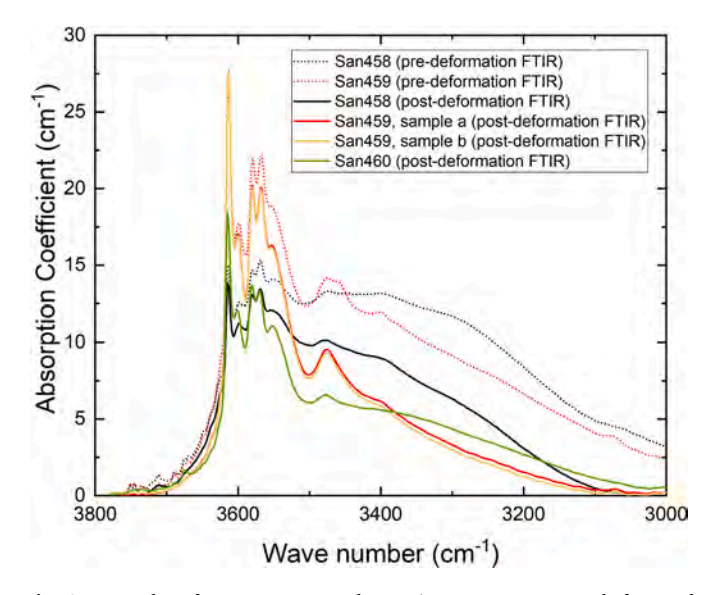


**Fig. 1.** Examples of FTIR spectra used to estimate water content before and after deformation experiments. The samples with the largest grain size retained the least amount of water, while the samples with the smallest grain size contain the highest amount of water. FTIR absorption spectra show sharp peaks in  $3500-3600~{\rm cm}^{-1}$  together with broader absorption in  $3500-3200~{\rm cm}^{-1}$  suggesting that a majority of water in these samples are OH in the crystalline lattice (and perhaps at grain-boundaries). The strength of absorption is reduced somewhat after deformation, but the degree of reduction is small (~30%).

The pre-deformation grain size of all samples is summarized in Table 1.

The representative samples (1 mm diameter) from each hot-pressed batch were also polished to the thickness of  $\sim\!100\,\mu m$ . The water content was determined by Fourier Transform Infrared Spectroscopy (FTIR) using Excalibur FTS 3000 with UMA 600 Microscope. The collected spectra were analyzed between 3000 and 3700 cm $^{-1}$ , corresponding to absorption bands generally associated with hydrogen in olivine. The background correction was done using the spline function, and the hydroxyl concentration was calculated from the corrected infrared spectra by integrating the area under the hydroxyl bands using Paterson (1982) calibration. FTIR analysis of our samples showed a substantial amount of water ( $\sim\!1000$  ppm wt for hot-pressed samples and 600–800 ppm wt for deformed samples) (Fig. 1, Tables 1 and 2). This is presumably from adsorbed water in our ultra-fine-grained starting materials. General uncertainties in water content are estimated up to  $\sim\!10\%$ .

We also measured grain size of the samples after each deformation experiments (those values are reported in Table 2).

# 2.3. Sample assembly and configuration

We followed the approach of the cell configuration and sample assembly that were given by Girard et al. (2020) (Fig. 2a). Both San Carlos and solgel samples were emplaced symmetrically relative to the center of the cell, separated by the pyrope and platinum discs. The pyrope acts as a stress sensor providing additional data on stress while Pt discs

Table 2

Deformation experiments results. Pressure and temperature errors come from pyrope and Pt EOS. Uncertainties in stress are derived from difference between individual hkl stresses.

Deformation run	P (GPa)	T (K)	Sample	Deformation step	Final stress (MPa)	Strain rate x $10^{-6}$ (s <sup>-1</sup> )	Final grain size (μm)	Final Water C <sub>OH</sub> (ppm wt)
San457 3.0		1014 ±	San Carlos (K1984)	1st 2nd	$\begin{array}{c} 22\pm5\\ 43\pm5 \end{array}$	$6.9 \pm 0.7 \ 14.2 \pm 1.4$	$0.37 \pm (0.21, 0.25)$	756 ± 75
	$3.0\pm0.3$	30	Solgel (K1981)	1st 2nd	$21 \pm 6$ $23 \pm 6$	$6.9 \pm 0.7$ $14.2 \pm 1.4$	$0.24 \pm (0.11, 0.18)$	$756\pm75$
San458 5.0	50101	973 ± 50	San Carlos (K1982)	1st 2nd	$131\pm9\\243\pm9$	$\begin{array}{c} 8.1 \pm 0.8 \\ 14.0 \pm 1.4 \end{array}$	$0.39 \pm (0.23, 0.29)$	$752\pm75$
	$5.0 \pm 0.4$		Solgel (K1976)	1st 2nd	$\begin{array}{c} 44\pm 8 \\ 110\pm 8 \end{array}$	$2.7 \pm 0.3 \ 8.6 \pm 0.9$	$0.27 \pm (0.14, 0.19)$	$752\pm75$
San459	10.0 $\pm$	1073 ± 45	San Carlos (K1982)	1st 2nd	$70\pm 9\\162\pm 9$	$4.7 \pm 0.5$ $8.7 \pm 0.9$	$0.77 \pm (0.48, 0.60)$	$735\pm73$
	0.7		Solgel (K1976)	1st 2nd	$\begin{array}{c} 31 \pm 8 \\ 47 \pm 8 \end{array}$	$\begin{array}{c} 2.7 \pm 0.3 \\ 11.1 \pm 1.0 \end{array}$	$0.31 \pm (0.16, 0.23)$	$735\pm73$
San460	$10\pm1$	1123 ± 80	San Carlos (K1982)	Single	$144 \pm 9$	$4.8 \pm 0.5$	$0.96 \pm (0.54, 0.70)$	$610\pm61$
	10 ± 1		Solgel (K1976)	Single	47 ± 9	$2.7\pm0.3$	$0.36 \pm (0.18, 0.26)$	$610\pm61$

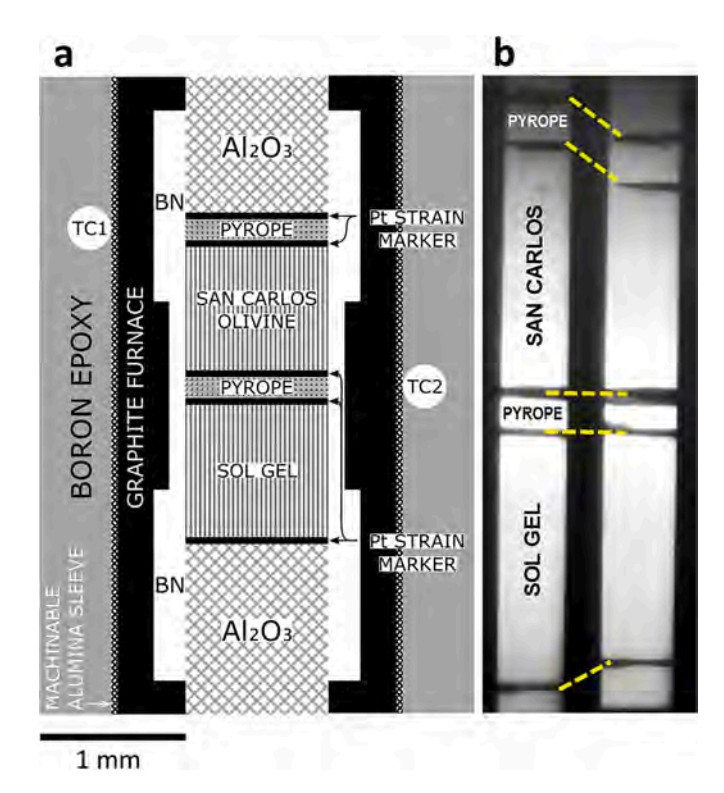


**Fig. 2.** a) The schematics of the experimental cell. b) Radiographic images used for calculation of strain rate (before (left) and after deformation (right)). Platinum foil was used as strain markers.

ensure radiographic contrast (strain marker) during the synchrotron deformation experiments (Girard et al., 2020). We note that in contrast to deformation experiments in the dislocation creep regime where the diffraction plane dependence of lattice strain is very large, the use of a pyrope stress sensor is not essential in our case, because, as we will show, diffraction plane dependence of lattice strain is small in case a sample deforms by diffusion creep. Also, because temperature is so low that pyrope deformed elastically and its strain was too small to be measured reliably (see Fig. S2). Pt discs, combined with pyrope, were also used to determine pressure and temperature from the equation of state (EOS) (discussed in Section 2.4). The olivine samples were surrounded by pyrope disc and machinable alumina on the periphery which acts as a load transmitting medium. This column was emplaced in boron

nitride (BN) sleeve which in turn was surrounded by a graphite stepped furnace (consisting of three separate components and assembled separately) to minimize temperature gradient in a sample assembly. Methods of temperature estimates will be discussed in the next section.

### 2.4. Experimental procedure and the error estimates

All deformation experiments were performed using a D-DIA apparatus (Wang et al., 2003) at the 6-BM-B white X-ray beamline at Advanced Photon Source (APS) in Argonne National Laboratory. The lists of runs, as well as experimental details associated with each experiment are given in Table 2. The sample cell assembly was emplaced in D-DIA and the X-ray beam calibration was conducted before compression. Subsequently, the experimental cell assembly was compressed to a target pressure. During cold compression, stress was monitored using radial X-ray diffraction of the samples, D-DIA differential rams were retracted to maintain differential stress to a minimum (typically less than ~10 MPa) and ensure nearly hydrostatic conditions. After reaching pressure, the temperature was raised to the target value (further decreasing the stress in the sample), and deformation was initiated after 15 min (time needed to collect high P-T spectra). This approach was chosen instead of typical annealing to minimize the grain growth which was essential for the success of these experiments.

The deformation experiments (and collection of diffraction spectra) were conducted by advancing one anvil relative to another opposite anvil with a fixed advancement rate. Deformation experiments were made to strain generally exceeding 10% axial strain. Because we have two samples in a given sample assembly, we needed to determine the strain of each sample separately. The strain of each sample was determined from the X-ray radiography images that were collected every 15 min. The uncertainty in strain determined from the radiographic images depends on the pixel size of the image relative to the sample thickness and the quality of the image. The pixel size 2  $\mu$ m in the present study corresponds to the resolution of strain of 0.5% for a sample of 400  $\mu$ m thickness. If the total strain is 5% this corresponds to an error of ~10% in strain rate. However, if the total strain is small (this is a case for pyrope), strain measurements have a larger uncertainty.

Once samples reached above  $\sim$ 5% strain, the strain rate was changed (doubled). Strain ( $\varepsilon$ ) was calculated by measuring the change in sample length (l- $l_0$ ) (outlined by strain markers shown in Fig. 2b) in radiographic images taken throughout the deformation:

$$\varepsilon (\%) = \frac{(l - l_0)}{l_0} \times 100 \tag{1}$$

Stress was estimated from radial X-ray diffraction performed on each

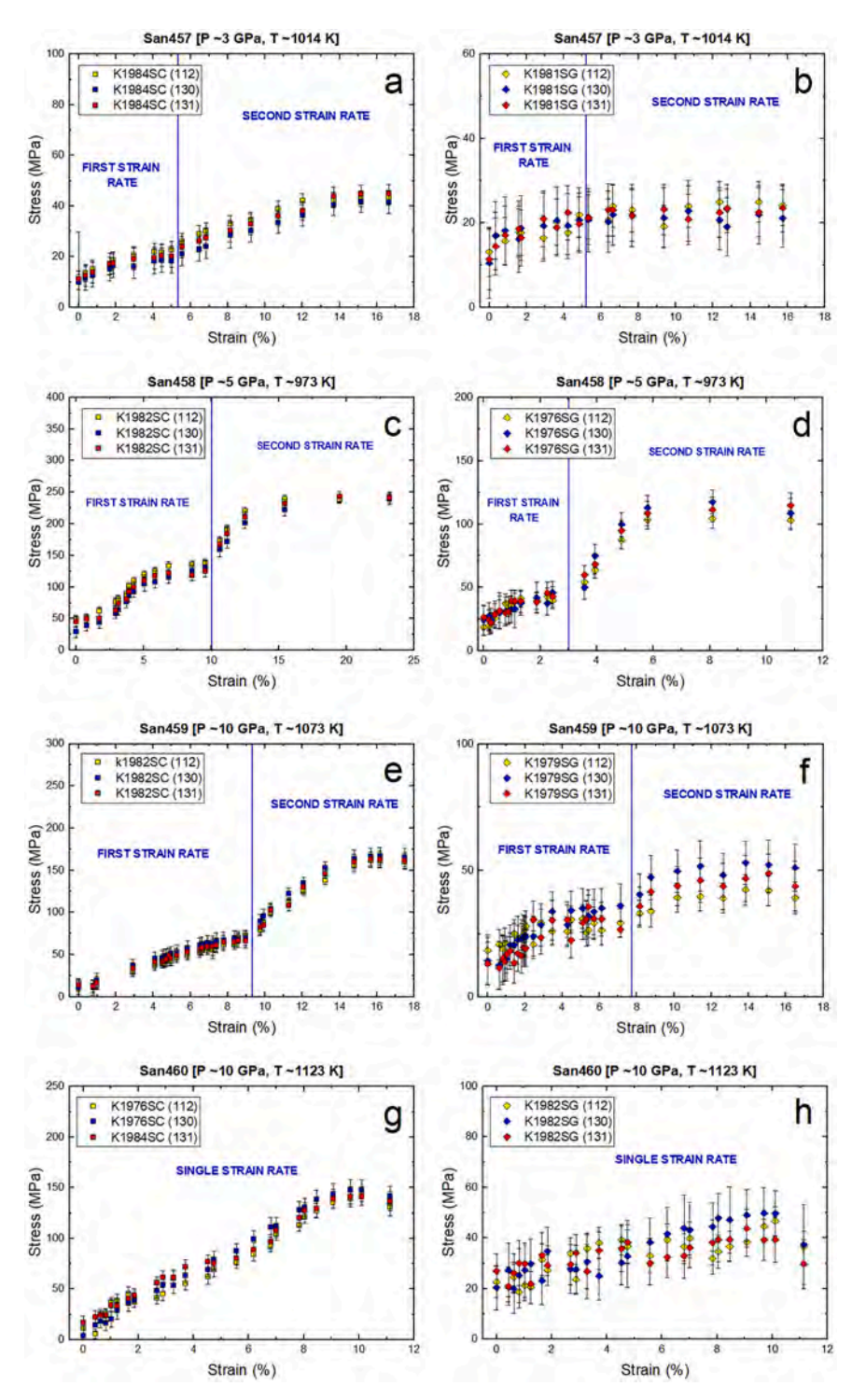


Fig. 3. Plots of differential stress vs. strain for all deformation experiments. For clarity, San Carlos (left panels) and solgel (right panels) are plotted separately. The vertical blue lines in panels a-f represent the strain at which we doubled the strain rate during deformation experiments. (For interpretation of the references to colour in this figure legend, the reader is referred to the web version of this article.)

sample as well as stress sensors. Energy dispersive X-ray diffraction data were collected with a constant 20 collected using a set of nine detectors located at equally spaced azimuthal angles (between  $0^{\rm o}$  and  $180^{\rm o}$  vertical detectors). The diffracted X-rays were collected at each azimuthal angle and were used to estimate the lattice strain. The lattice strain is subsequently used to calculate the differential stress  $\sigma_{\rm hkl}$  for the particular (hkl) reflection in crystals during deformation based on earlier work by Singh (1993):

$$d_{hkl}(\psi) \propto d_{hkl}^0 \left\{ 1 + \frac{\sigma_u}{6M} \left( 1 - 3\cos^2 \psi \right) \right\}$$
 (2)

where  $d_{hkl}$  is the d-spacing for the lattice plan (hkl),  $d^0_{hkl}$  is the d-spacing in hydrostatic conditions for the lattice plan (hkl), M is the Voigt-Reuss-Hill average of shear modulus,  $\psi$  is the azimuthal angle, and  $\sigma_{u}$  is the uniaxial stress applied on the material that we want to estimate. Stress is estimated by fitting the  $d_{hkl}(\psi)$  (Fig. S3). Further details were previously described by Li et al. (2004), Li et al. (2006), Vaughan et al.

#### (2000) and Dixon and Durham (2018).

Note that the relation (2) is valid when the material is plastically isotropic (Karato, 2009). When a material is plastically anisotropic, stress estimated from this relation becomes strongly sensitive to diffraction plane (hkl). The experimental observations from our present study demonstrate weak (hkl) dependence of stress, as will be shown later, and we can justify the use of this relation to estimate the stress acting on the sample.

Pressure and temperature were estimated from the change in the molar volume determined by X-ray diffraction of pyrope and platinum, using the equations of state (EOS) for these materials under the hydrostatic conditions before the anvil was advanced to provide a differential stress. This was done by plotting the P and T calculated from EOS of platinum (Zha et al., 2008; Matsui et al., 2009) and pyrope (Zou et al., 2012; Hu et al., 2016; Fan et al., 2017) using corresponding thermodynamic parameters. The point in P-T space where the lines corresponding to platinum and pyrope intersect represents the experimental pressure and temperature (with corresponding uncertainties). The uncertainties in pressure come from the uncertainties in the estimate of the molar volume of a sample by X-ray diffraction and from the uncertainties in the equation of state including thermal expansion. The pressure estimated from the molar volume also depends on temperature and using two materials we can determine both pressure and temperature. Therefore, pressure uncertainty comes directly from the uncertainty in molar volume estimated from X-ray diffraction collected at hydrostatic conditions at high pressure and high temperature (just before deformation).

Temperature estimate is more challenging. Two issues must be analyzed. The first is the estimate of the absolute values of temperatures, and the second is the temperature gradient in a sample. We use four methods to address these issues: (i) the power-temperature relationships established for a sample assembly similar to ours (as a guide to reach a certain temperature), (ii) readings from two thermo-couples (one near the center and another is located near the top corner of a cube), (iii) molar volumes of two materials in a sample assembly, and (iv) finite element modeling of temperature distribution in a sample assembly (we used a program developed by Hernlund et al., 2006). Combining these results, we estimate that the temperature variation in a sample is ~20 K and the errors in the absolute temperature is ~50 K (this depends on a particular run (see Table 2)). Pressure and temperature estimates and their respective uncertainties are reported in Table 2.

The errors in stress are less trivial and required a more subtle approach. Stress was determined from the analysis of radial X-ray diffraction, and was calculated on each sample, using the theory of Singh (1993). However, stress was also measured from a stress sensor. To determine stress in olivine, we used the best observed diffraction peaks obtained from primarily (130), (131) and (112) planes. For pyrope, we used (420), (332), (422) and (431) planes. Plot85, an energy-dispersive peak fitting software package developed at the Mineral Physics Institute at Stony Brook University (http://www.mpi.stonybrook.edu/NSLS/X1 7B2/Support/Plot85/plot85.htm), was used to process the diffraction peaks. To reduce uncertainties calculated in peak fitting, the individual peaks were manually analyzed. While this approach is extremely time consuming, it is necessary in obtaining well-constrained stress values and very low stress uncertainties (generally within  $\pm 10$  MPa). Note that the uncertainties in stress measurements are not the percentage of estimated stress but are determined by the resolution of stress. Consequently, the relative errors are larger for a case where the sample is weak.

As will be reported in the next section, stresses in stacked samples are not always similar. In some cases, stress values differ largely. We will provide a model to explain such an observation in terms of the influence of constraints on deformation.

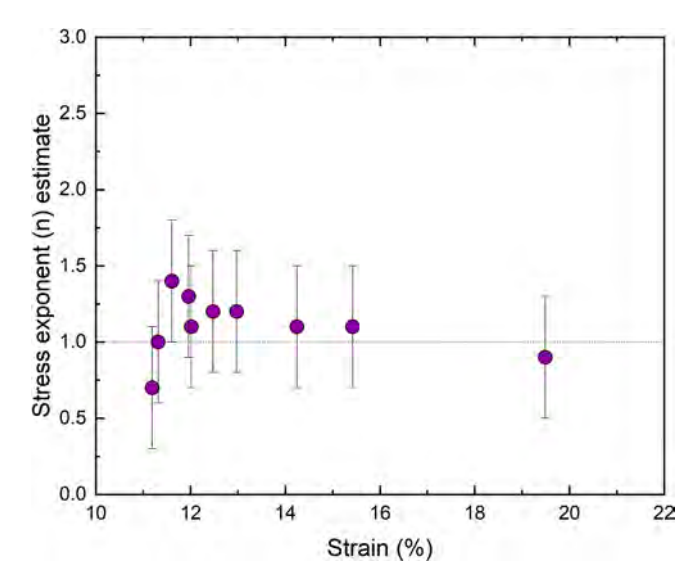


**Fig. 4.** The example measured stress exponent from San458 (San Carlos; 2nd strain rate). The stress exponent is calculated from two data points, one just before the change in strain rate, and another is after the change to a new strain rate at various strain. The stress exponent approaches unity in all our experiments, within given uncertainties.

#### 3. Results

### 3.1. Mechanical data and the inference of deformation mechanism

Typical stress-strain curves are shown in Fig. 3a-h. In these figures, we do not show the results from pyrope because the strain of pyrope is so small that we could not determine strain with acceptable precision (in Fig. S2, we show stress of pyrope as a function of time). This is not a major problem in this case, because the stress of each sample is not strongly dependent on the diffraction plane (hkl).

A common method to infer the mechanisms of deformation is to determine the stress and grain size sensitivity of strain rate. In this approach, we use the following relation  $\dot{\varepsilon}=A\cdot\sigma^n\cdot d^{-m}$  ( $\dot{\varepsilon}$ : strain rate,  $\sigma$ : stress, d: grain size) and determine n and m, and infer the mechanism of deformation. However, estimating m is almost impossible from our own data because of a small grain size range and of large uncertainties in the stress and strain estimate. For the stress exponent (n), we could estimate it from some runs. An example is shown in Fig. 4. The results  $n\sim 1.0\pm 0.5$  is consistent with diffusion creep. However, the estimate of stress exponent (n) is difficult due to the large uncertainties in the estimates of stress and strain. Therefore, we also used the following qualitative or semi-quantitative observations from our results to infer the operation of diffusion creep:

- (i) For the temperature (and pressure) and strain rate used in our experiments, the stress measured in our samples ( $\sim$ 20–250 MPa depending on the conditions) is substantially smaller than the stress expected for dislocation creep (for dislocation creep, when T=1100 K and P=5 GPa, strain rate  $=10^{-5}$  s<sup>-1</sup>, stress will be  $\sim$ 10 GPa (estimated from Karato and Jung (2003) and Kawazoe et al. (2009)), indicating that the samples in our experiments deform by a mechanism other than dislocation creep,
- (ii) the stress estimated from the lattice strain is nearly independent of diffraction planes (hkl), and.
- (iii) there is evidence of time hardening.

By combining these observations with a rough estimate of the stress exponent, we infer the operation of diffusion creep in our samples (see more detailed discussion in Section 4).

Generally, solgel olivine shows substantially smaller strength than

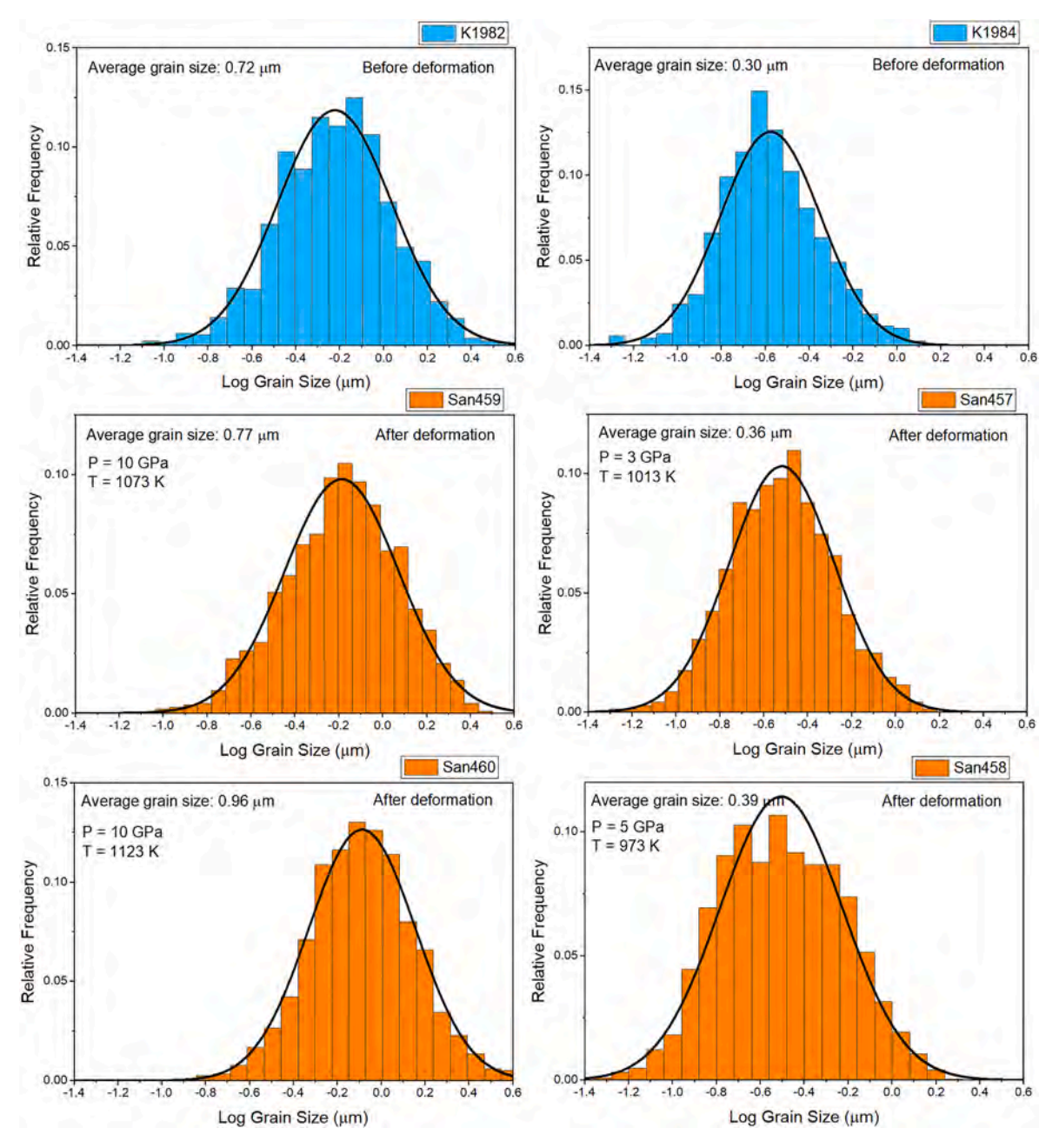


**Fig. 5.** Distribution of the grain sizes from two different aggregates of San Carlos parent samples (blue) compared with the grain size distribution after the deformation experiments (orange) at given pressure and temperature conditions. For all panels, the number of measured grain intercepts is in the range between 1000 and 2000. (For interpretation of the references to colour in this figure legend, the reader is referred to the web version of this article.)

San Carlos olivine. This is largely due to the fact that solgel olivine has a substantially smaller grain size than San Carlos olivine in our study.

# 3.2. Estimation of activation volume

From the results summarized above, we conclude that diffusion creep operates in our samples. Therefore, we use the following constitutive equation to determine the activation volume  $V^*$ :

$$\dot{\varepsilon} = A\sigma d^{-m}C_W^r \exp\left(-\frac{E^* + PV^*}{RT}\right) \tag{3}$$

where  $\dot{\varepsilon}$  is strain rate,  $\sigma$  is stress, d is grain size, m is a non-dimensional constant (m=2 or 3),  $C_W$  is water content (ppm wt), r is a non-dimensional constant (r=0.7-1; Mei and Kohlstedt, 2000a),  $E^*$  is activation energy ( $E^*=295$  J/mol (Mei and Kohlstedt, 2000a)),  $V^*$  is

activation volume, P is pressure, T is temperature, and R is the gas constant.

Because we have the experimental data under the broad range of pressure (from 3 to 10 GPa from this study, but we also have previous results at lower pressures), we can obtain strong constraint on  $V^*$ . However, several issues need to be examined in estimating  $V^*$  from our experimental observations. First, because of time-hardening, none of our data represents true steady-state deformation. This is a common observation for diffusion creep where grain growth must occur during deformation leading to time-hardening (e.g., Karato et al., 1986; Mohiuddin et al., 2020). However, using the results of previous study such as Karato et al. (1986) and a theoretical basis based on Raj and Ashby (1971), we believe that the influence of transient creep is small (see the Discussion section for the details). Second, both water content and grain size changed during a single run (Figs. 1, 5, 6; Tables 1, 2).

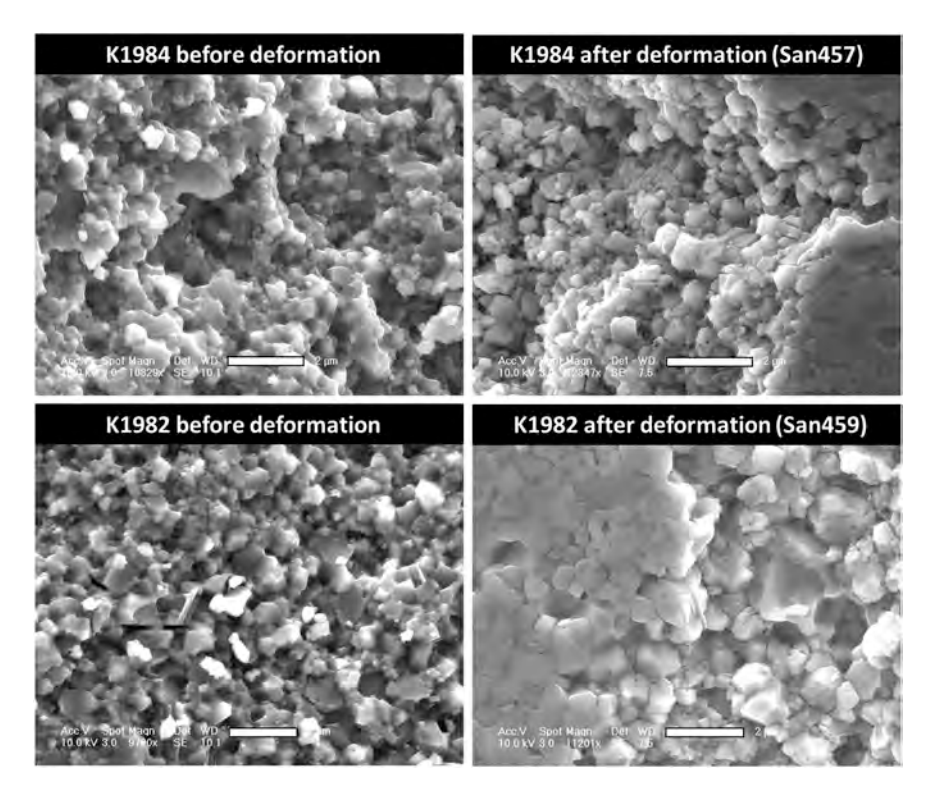


Fig. 6. Example of microstructure (grain size) observed in initial samples and the recovered samples. The scale bar in all images is 2 µm.

Although the influence of these factors is relatively small (water content changed  $\sim\!30\%$ , grain size increased  $\sim\!20{\text -}50\%$ ), corrections on these factors need to be made. Third, in many experiments, not only pressure but also other factors are different including grain size, temperature, stress and water content. Therefore, we determine  $V^*$  by comparing various data collected at a broad range of conditions after normalization, where we normalized all parameters other than pressure to common values, and determine  $V^*$  using the relation:

$$V^* = -RT \frac{\partial log\dot{\varepsilon}(T_0, d_0, \sigma_0, C_{w0})}{\partial P}$$
 (4)

where  $\dot{\epsilon}(T_0,d_0,\sigma_0,C_{w0})$  is the normalized strain rate and  $T_0$ ,  $d_0$ ,  $\sigma_0$ ,  $C_{w0}$  are the normalization temperature ( $T_0=1000~\rm K$ ), normalization grain size ( $d_0=1~\rm \mu m$ ), normalization stress ( $\sigma_0=50~\rm MPa$ ) and normalization water content ( $C_{w0}=1500~\rm ppm$  wt), respectively. Temperature effect was corrected using the activation energy of 295 kJ/mol (in principle, we need  $V^*$  to make this correction (because activation enthalpy ( $H^*$ ) include activation volume ( $H^*=E^*+PV^*$ )), but compared to the uncertainties in  $E^*$ , the  $PV^*$  term can be ignored). Grain size effect was corrected using  $T=0.7-1.0~\rm Mei$  and Kohlstedt, 2000a). We evaluated  $V^*$  by the weighted least squares method including the uncertainties of each data (Fig. 7).

Regarding the changing water content during a run, we used average water content to represent a water content for a run. Since water content changed only modestly, we believe that this is justifiable. For grain size, we use initial and final grain size and estimated grain size during a run, by interpolating these grain sizes using a grain growth law. Again, the degree of grain growth is limited in our study (because of low temperatures and the use of pinning materials to minimize grain growth), we believe that this approximate approach is justifiable.

Table 3 shows the results for estimated activation volume, obtained from linear regression of our data alone, assuming r=0.7 or 1, m=2 or 3 (Fig. 7). We conclude that  $V^*\sim 2.5\pm 0.6$  cm³/mol for both San Carlos and solgel olivine (in this study we do not observe major difference in rheological properties of San Carlos and solgel olivine).

For the purpose of comparison with low P data available in literature, we have overlaid data from Mei and Kohlstedt (2000a), normalized to the same T and grain size in Fig. 7. Their strain rates for 100, 300 and 450 MPa, after being corrected for the influence of different grain size and temperature, show consistency with our own normalized strain rate (Fig. 7). However, we did not use Mei and Kohlstedt (2000a) data in linear regression toward estimating  $V^*$  because this would produce large uncertainties caused by large extrapolation in grain size and temperature. Nevertheless, the close agreement of the Mei and Kohlstedt (2000a) data at low P to the expected P dependent trend in our strain rate data (when m=3 is assumed) is an additional supporting evidence for the diffusion creep mechanism in our experiments.

#### 4. Discussions and conclusions

In most of the previous studies, the operation of deformation mechanism is made mainly by the experimentally determined values of the stress exponent (n) and grain size exponent (m). Observations of  $n \sim 1$  and  $m \sim 2-3$  (or non-zero m) are used to conclude the operation of diffusion creep (e.g., Karato et al., 1986; Mei and Kohlstedt, 2000a). In the present study, we also determined the stress exponent n (Fig. 4), but uncertainties in the estimated values of n are large due to the uncertainties in the grain size estimate (in order to estimate n we need to make a correction for grain growth) and to the relatively large uncertainties in the stress estimates particularly at a low stress level (from some runs n can be estimated to be near n (Fig. 4) but n is unconstrained because grain size range is small).

Therefore, we also use other more robust observations to conclude that the samples deformed by diffusion creep including (i) the near independence of lattice strain on the diffraction planes (hkl) (in Section 3.1), (ii) the much lower strength of samples than the strength expected for dislocation creep. However, the validity of using these indirect observations to infer the operation of diffusion creep needs to be examined in detail. For example, the near independence of lattice strain on diffraction planes could well be due to elastic deformation (Karato, 2009). However, the possibility of elastic deformation can be ruled out

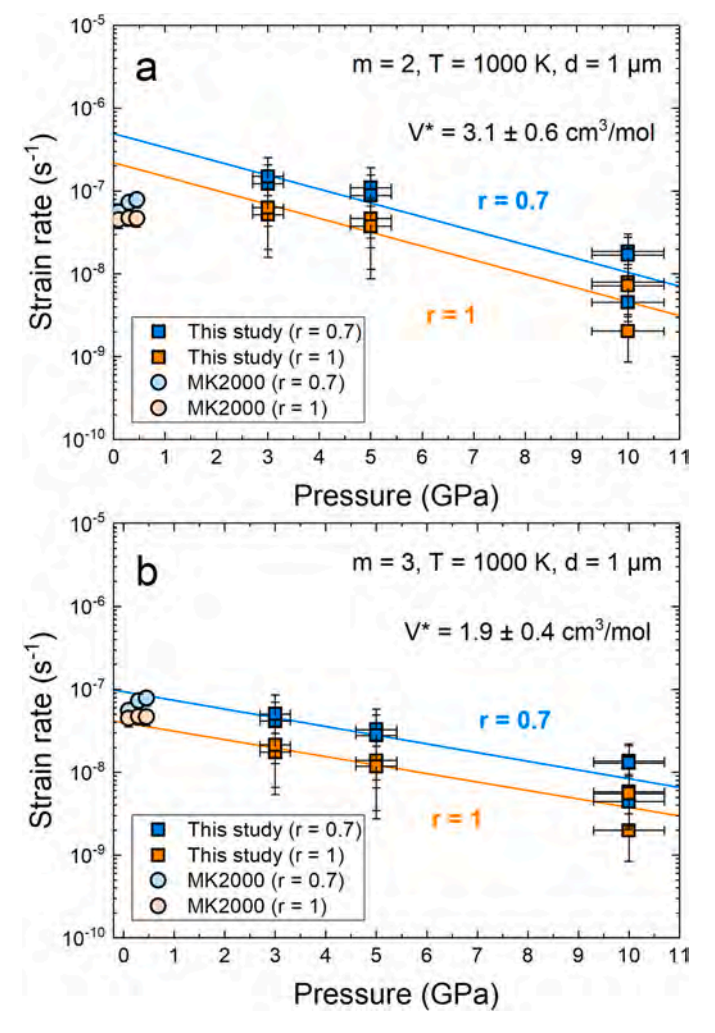


Fig. 7. Example of linear regression analysis using only our data, to obtain the activation volume ( $V^*$ ). Prior to the regression, data were normalized to a common temperature ( $T=1000~\rm K$ ) using activation energy of 295 kJ/mol, and common grain size ( $d=1~\rm \mu m$ ) using grain size exponents ( $m=2~\rm (a)$  or 3(b)) and common stress of 50 MPa using stress exponent n=1. We also normalized water effect to a common water content of 1500 ppm wt using  $r=0.7~\rm (blue)$  or  $r=1~\rm (orange)$ . We have added Mei and Kohlstedt (2000a) data, normalized to the same T and the grain size for the purpose of comparison with low P data, however we do not use it in linear regression fit to estimate  $V^*$ . (For interpretation of the references to colour in this figure legend, the reader is referred to the web version of this article.)

because stress we expect for elastic deformation far exceeds what we observed (for elastic deformation, we should expect stress from  $\sigma=M\varepsilon$  (where  $\sigma$  is stress, M is the elastic modulus, and  $\varepsilon$  is strain). Using the

value of M=200 GPa (Young's modulus), we get  $\sigma\sim 20$  GPa at 10% strain that is far above the observed stress. Thus we conclude that our samples deform by diffusion creep.

Another observation that needs some explanation is that strain (strain rate) and stress in two samples in a single sample assembly are often different (e.g., Fig. 3c, d). If two samples are stacked in series in a compression test, one might expect the same stress but different strain (rate) in two stacked samples. A key to understand this is to realize that samples in the D-DIA do not deform freely but their deformation is constrained by the surrounding materials. A theory is developed to analyze the influence of constraints on sample stress and strain (Supplementary Material).

The essence of the theory is that when two specimens are stack together and compressed uniaxially (by applying the normal stress  $\sigma_1$  (with the lateral stress of  $\sigma_3$ )) without any lateral constraints, then both  $\sigma_1$  and  $\sigma_3$  will be same for these two samples, and one expects that  $\sigma_1 - \sigma_3$  will be same for the two samples. However, when samples are surrounded by a material with some strength, the finite strength of the surrounding material provide different  $\sigma_3$  to the sample that depends on the strength contrast between the sample and the surrounding material.

This theory shows that when samples are weak compared to the strength of the surrounding materials, the influence of constraints is large. Consequently, the strain in each sample will be similar in this case, leading to different stress among different samples (e.g., run San457). In contrast, when samples are stronger than the surrounding materials, constraints are weak and we will observe different strains but similar stresses among stacked samples (e.g., run San458). Despite this complication, the measured stress and strain rate are stress and strain rate of a sample itself, and consequently, the measured results can be used to determine the plastic properties of a sample without the need to make corrections on the degree of constraints.

Note, however, that the influence of constrained deformation causes a limitation to which a stress sensor may work. An implicit assumption behind the stress sensor was that stress in stacked samples is the same (Girard et al., 2020). Our present results show that this is not the case when samples (and a stress sensor) are weaker than the surrounding material (pressure medium).

Common to many laboratory studies on diffusion creep, we noted time-hardening presumably caused by concurrent grain-growth (e.g., Karato et al., 1986; Mohiuddin et al., 2020). There is no true steady-state in our study, and we need to examine the importance of transient creep. For two different reasons, we consider that the influence of transient creep is not important. Karato et al. (1986) observed substantial time-hardening caused by grain-growth, and interpreted those data using the data on grain-growth. They also reported results showing less time-hardening from which they determined the nearly steady-state rheology for diffusion creep. The strength from these two sets of data is indistinguishable suggesting that transient creep is not important. This can be explained based on the model of transient diffusion creep. For diffusion creep, the most important cause of transient creep is the variation in stress distribution at grain-boundaries (Raj and Ashby, 1971). When

Table 3 Activation volume and pre-exponential factor A obtained using the general least squares method of our data alone permuted to different normalization parameters and assuming r = 0.7 or 1 and m = 2 or 3.

r	m	T (K)	d (μm)	Stress (MPa)	C <sub>OH</sub> (ppm wt)	Α	Error in A	V* (cm <sup>3</sup> /mol)	Error in V* (cm <sup>3</sup> /mol)
San Car	los								
0.7	2	1000	1	50	1500	45,862	28,800	3.1	0.6
0.7	3	1000	1	50	1500	19,353	8616	1.9	0.4
1	2	1000	1	50	1500	2131	1277	3.1	0.5
1	3	1000	1	50	1500	899	377	1.9	0.4
Solgel									
0.7	2	1000	1	50	1500	51,305	46,045	3.2	0.7
0.7	3	1000	1	50	1500	21,975	14,835	2.4	0.6
1	2	1000	1	50	1500	2384	2074	3.2	0.7
1	3	1000	1	50	1500	1021	669	2.4	0.6

stress is applied to a polycrystalline sample, stress across the grain-boundaries evolves from that determined by elastic accommodation with sharp stress concentration to the one determined by diffusional accommodation with smooth stress distribution. This large change in stress distribution (i.e., stress gradient) occurs in the initial stage of deformation where the mechanism of accommodation changes from elastic to diffusional accommodation. During the later stage of deformation with continuously changing grain size, stress distribution on grain-boundaries is always determined largely by diffusional accommodation. Therefore, we do not expect any substantial transient effect caused by concurrent grain-growth.

Since we added fine-grained  $Al_2O_3$  powder to minimize grain growth, there is a possible influence of  $Al_2O_3$  on diffusion. However, when our data are compared with the data on San Carlos olivine by Mei and Kohlstedt (2000a) with the grain size exponent of m=3, they agree well (see Fig. 7) indicating that the influence of  $Al_2O_3$  is small. This is likely due to the fact that natural olivine is in equilibrium with the  $Al_2O_3$ -bearing phase such as spinel or garnet and hence contains some  $Al_2O_3$ .

Results of studies on the pressure effects on diffusion may be compared with our results. Misener (1974) reported the activation volume of ~6 cm<sup>3</sup>/mol for Mg—Fe diffusion in San Carlos olivine. Béjina et al. (1999) reported  $V^* \sim 0.7 \pm 2.3$  cm<sup>3</sup>/mol for Si diffusion in San Carlos olivine. Small values of  $V^*$  reported in these studies are similar to our results, but the water content in the samples was not measured in these studies which makes its interpretation difficult (water is likely dissolved in olivine at high pressures, and if the water content changes that takes place with pressure is not properly quantified, then the true pressure effects cannot be determined). Another related study is a study on the pressure effects on grain-growth in olivine (Zhang and Karato, 2021) who obtained  $V^* \sim 5$  cm<sup>3</sup>/mol. Grain-growth involves grainboundary diffusion, so one may expect a similar  $V^*$  for grainboundary diffusion creep and grain-growth. Somewhat smaller  $V^*$ from our study may be caused by water because Zhang and Karato's samples contained substantially smaller amount of water (< 50 ppm wt).

We may compare our results by those reported by Nishihara et al. (2014). In their experiments, conditions for deformation were close to the boundary between diffusion creep and other mechanisms of flow such as grain-boundary sliding accommodated by dislocation creep. Consequently, they estimated the flow law parameters for diffusion creep through the least square data fitting assuming n=1 for one mechanism (diffusion creep), and estimated the activation volume of 8.2  $\pm$ 0.9 cm<sup>3</sup>/mol. This is substantially larger than our result, and the cause of this difference is unclear. Possibilities include: (i) our study was under the water-rich conditions whereas the study of Nishihara et al. (2014) was under the water-poor conditions, and/or (ii) their estimated value of  $V^*$  may be influenced by the activation volume for another mechanism.

#### 5. Summary and geophysical implications

Using small grain size specimens, we report the first experimental results on the pressure effects on diffusion creep in wet olivine. Much higher values of activation volume ( $V^*$ ) for diffusion creep in olivine were reported:  $\sim 15~{\rm cm}^3/{\rm mol}$  by Mei and Kohlstedt (2000a) by low pressure experiments ( $< 0.45~{\rm GPa}$ ) and  $\sim 20~{\rm cm}^3/{\rm mol}$  by Jain and Korenaga (2020) based on numerical analysis of very limited experimental data in comparison to the geodynamic modeling calculations of seismic anisotropy. Our observations clearly rule out such high values of  $V^*$  and demonstrate the importance of laboratory studies under high pressures.

In contrast, activation volume for dislocation creep in olivine is substantially higher,  $\sim 15~{\rm cm}^3/{\rm mol}$  (Karato and Rubie, 1997; Kawazoe et al., 2009; Karato and Jung, 2003; Dixon and Durham, 2018). A small activation volume compared to that for dislocation creep implies that diffusion creep will play an important role in the deep upper mantle.

Because deformation mechanisms (either dislocation or diffusion creep) have important influence for the formation of anisotropic structure such as lattice-preferred orientation (LPO), processes generating LPO and hence seismic anisotropy in the deep upper mantle need to be evaluated in detail incorporating our new result. Toward that goal, a few issues need to be studied in more comprehensively.

First, variation of dominant mechanisms of deformation in Earth depends on how stress (or strain rate) is distributed which in turn depends on the boundary conditions for mantle flow. The nature of stress, strain distribution depends on the boundary conditions and likely differ among different geological setting.

Second, in a broad region of Earth's upper mantle, expected conditions are close to the mechanism boundary as pointed out by Karato et al. (1986) and Karato and Wu (1993). When a material deforms under the conditions close to the mechanism boundary, a delicate interplay of diffusion and dislocation creep takes place near the mechanism boundary. The experimental studies on calcite (Pieri et al., 2001; Walker et al., 1991) and perovskite (Karato et al., 1995) show that when a material deforms in the diffusion creep regime close to the mechanism boundary, strong lattice preferred orientation (LPO) develops, but if the same material deforms in the diffusion creep regime far from the mechanism boundary, LPO is nearly random.

Third, the dominant deformation mechanism strongly depends on grain size. Processes controlling grain size (e.g., dynamic recrystallization, grain-growth) need to be investigated in more detail particularly under the deep upper mantle conditions.

Forth, in evaluating the competition between diffusion and dislocation creep, it is important to examine the possible role of change in the controlling slip system in dislocation creep (e.g., Masuti et al., 2019). Such subtleties are important because expected conditions in the upper mantle are close to the regime boundary between diffusion and dislocation creep.

Exploring these issues is beyond the scope of this paper, but our new experimental results on the pressure effects on diffusion creep in wet olivine provide a basis for such studies.

#### Credit statement

Reynold Silber and Jennifer Girard conducted experiments, analyzed and processed data and wrote parts of the manuscript. Shun Karato wrote parts of the manuscript and advised on key aspects of the work.

#### **Declaration of Competing Interest**

The authors declare no conflict of interest.

# Acknowledgements

The authors thank the two anonymous reviewers for their comments and suggestions that helped improve this paper. This research is supported by the National Science Foundation (EAR-1818792). RES thanks the Banting Postdoctoral Fellowship (Natural Sciences and Engineering Research Council of Canada) program administered by the Government of Canada for supporting this research. The authors thank Haiyan Chen, the beamline scientist at 6-BM-B at APS, for her help during experiments and with cell assembly testing that is supported by the U.S. Department of Energy (DOE) and the Consortium for Materials Properties Research in Earth Sciences (COMPRES). All data are provided in the main text and the Supplemental Material.

### Appendix A. Supplementary data

Supplementary data to this article can be found online at https://doi.org/10.1016/j.pepi.2022.106840.

#### References

- Abrams, H., 1971. Grain size measurement by the intercept method. Metallography 4, 59-78
- Béjina, F., Jaoul, O., Liebermann, R.C., 1999. Activation volume of Si diffusion in San Carlos olivine: implications for upper mantle rheology. J. Geophys. Res. 104, 25529–25542.
- Cahn, J., Fullman, R., 1956. On the use of lineal analysis for obtaining particle size distribution functions in opaque samples. J. Metals 8.
- Chen, J., Inoue, T., Weidner, D.J., Wu, Y., Vaughan, M.T., 1998. Strength and water weakening of mantle minerals, olivine, wadsleyite and ringwoodite. Geophys. Res. Lett. 25, 575–578.
- Darot, M., Gueguen, Y., 1981. High-temperature creep of forsterite single crystals. J. Geophys. Res. 86, 6219–6234.
- Dixon, N.A., Durham, W.B., 2018. Measurement of Activation Volume for Creep of Dry Olivine at Upper-Mantle Conditions. J. Geophys. Res. Solid Earth 123, 8459–8473.
- Durham, W.B., Mei, S., Kohlstedt, D.L., Wang, L., Dixon, N.A., 2009. New measurements of activation volume in olivine under anhydrous conditions. Phys. Earth Planet. Inter. 172, 67–73.
- Fan, D., Lu, C., Xu, J., Yan, B., Yang, B., Chen, J., 2017. Effects of water on PVT equation of state of pyrope. Phys. Earth Planet. Inter. 267, 9–18.
- Farla, R.J.M., Karato, S., Cai, Z., 2013. Role of orthopyroxene in rheological weakening of lithosphere via dynamic recrystallization. Proc. Nat. Acad. Sci. United States 110, 16355–16360.
- Faul, U.H., Jackson, I., 2007. Diffusion creep of dry, melt-free olivine. J. Geophys. Res. Solid Earth 112.
- Girard, J., Silber, R.E., Mohiuddin, A., Chen, H., Karato, S.-I., 2020. Development of a stress sensor for in-situ high-pressure deformation experiments using radial X-ray diffraction. Minerals 10, 166.
- Hernlund, J., Leinenweber, K., Locke, D., Tyburczy, J.A., 2006. A numerical model for steady-state temperature distributions in solid-medium high-pressure cell assemblies. Am. Mineral. 91, 295–305.
- Hirth, G., Kohlstedt, D., 2003. Rheology of the upper mantle and the mantle wedge: a view from the experimentalists. Geophys. Monograph-Am. Geophys. Union 138, 83–106.
- Hu, Y., Wu, Z., Dera, P.K., Bina, C.R., 2016. Thermodynamic and elastic properties of pyrope at high pressure and high temperature by first-principles calculations. J. Geophys. Res. Solid Earth 121, 6462–6476.
- Jain, C., Korenaga, J., 2020. Synergy of experimental rock mechanics, seismology, and geodynamics reveals still elusive upper mantle rheology. J. Geophys. Res. Solid Earth 125, e2020JB019896.
- Karato, S., 1992. On the Lehmann discontinuity. Geophys. Res. Lett. 19, 2255-2258.
- Karato, S., 2009. Theory of lattice strain in a material undergoing plastic deformation: Basic formulation and applications to a cubic crystal. Phys. Rev. B79 https://doi. org/10.1103/PhysRevB.1179.214106.
- Karato, S., Jung, H., 2003. Effects of pressure on high-temperature dislocation creep in olivine polycrystals. Philos. Mag. A. 83, 401–414.
- Karato, S.I., Rubie, D.C., 1997. Toward an experimental study of deep mantle rheology: a new multianvil sample assembly for deformation studies under high pressures and temperatures. J. Geophys. Res. Solid Earth 102, 20111–20122.
- Karato, S., Weidner, D.J., 2008. Laboratory studies of rheological properties of minerals under deep mantle conditions. Elements 4, 191–196.
- Karato, S., Wu, P., 1993. Rheology of the upper mantle: a synthesis. Science 260, 771–778.
- Karato, S., Paterson, M.S., Fitz Gerald, J.D., 1986. Rheology of synthetic olivine aggregates: influence of grain-size and water. J. Geophys. Res. 91, 8151–8176.
- Karato, S., Zhang, S., Wenk, H.-R., 1995. Superplasticity in Earth's lower mantle: evidence from seismic anisotropy and rock physics. Science 270, 458–461.

- Kawazoe, T., Karato, S., Otsuka, K., Jing, Z., Mookherjee, M., 2009. Shear deformation of dry polycrystalline olivine under deep upper mantle conditions using a rotational Drickamer apparatus (RDA). Phys. Earth Planet. Inter. 174, 128–137.
- Kohlstedt, D.L., Goetze, C., 1974. Low-stress, high-temperature creep in olivine single crystals. J. Geophys. Res. 79, 2045–2051.
- Li, L., Weidner, D., Raterron, P., Chen, J., Vaughan, M., 2004. Stress measurements of deforming olivine at high pressure. Phys. Earth Planet. Inter. 143, 357–367.
- Li, L., Weidner, D.J., Raterron, P., Chen, J., Vaughan, M.T., Mei, S., Durham, W.B., 2006. Deformation of olivine at mantle pressure using the D-DIA. Eur. J. Mineral. 18, 7–19.
- Masuti, S., Karato, S., Girard, J., Barbot, S., 2019. Anisotropic plasticity of olivine single crystals under wet conditions under the deep upper mantle conditions. Phys. Earth Planet. Inter. 290, 1–9.
- Matsui, M., Ito, E., Katsura, T., Yamazaki, D., Yoshino, T., Yokoyama, A., Funakoshi, K.-I., 2009. The temperature-pressure-volume equation of state of platinum. J. Appl. Phys. 105, 013505.
- Mei, S., Kohlstedt, D.L., 2000a. Influence of water on plastic deformation of olivine aggregates, 1. Diffusion creep regime. J. Geophys. Res. 105, 21457–21469.
- Mei, S., Kohlstedt, D.L., 2000b. Influence of water on plastic deformation of olivine aggregates, 2. Dislocation creep regime. J. Geophys. Res. 105, 21471–21481.
- Misener, D.J., 1974. Cationic diffusion in olivine to 1400° C and 35 kbar. In: Hofmann, A. W., Giletti, B.J., Yorder, H.S., J., Yund, R.A. (Eds.), Geochemistry and Reaction Kinetics. Carnegie Institution of Washington, Washington DC, pp. 117–129.
- Mohiuddin, A., Karato, S., Girard, J., 2020. Slab weakening during the olivine to ringwoodite transition in the mantle. Nat. Geosci. 13, 170–174.
- Nishihara, Y., Ohuchi, T., Kawazoe, T., Spengler, D., Tasaka, M., Kikegawa, T., Suzuki, A., Ohtani, E., 2014. Rheology of fine-grained forsterite aggregate at deep upper mantle conditions. J. Geophys. Res. Solid Earth 119, 253–273.
- Paterson, M.S., 1982. The determination of hydroxyl by infrared absorption in quartz, silicates glasses and similar materials. Bull. Mineral. 105, 20–29.
- Pieri, M., Kunze, K., Burlini, L., Stretton, I., Olgaard, D.L., Burg, J.-P., Wenk, H.-R., 2001. Texture development of calcite by deformation and dynamic recrystallization at 1000 K during torsion experiments of marble to large strains. Tectonophysics 330, 119–142.
- Raj, R., Ashby, M., 1971. On grain boundary sliding and diffusional creep. Metall. Trans. A. 2, 1113–1127.
- Ringwood, A.E., 1975. Composition and Structure of the Earth's Mantle. McGraw-Hill, New York.
- Singh, A.K., 1993. The lattice strains in a specimen (cubic system) compressed nonhydrostatically in an opposed anvil device. J. Appl. Phys. 73, 4278–4286.
- Vaughan, M., Chen, J., Li, L., Weidner, D., Li, B., 2000. Use of X-ray Imaging Techniques at High-Pressure and Temperature for Strain Measurements. AIRAPT-17, pp. 1097–1098.
- Walker, A.N., Rutter, E.H., Brodie, K.H., 1991. Experimental study of grain-size sensitive flow of synthetic, hot-pressed calcite rocks. In: Knipe, R.J., Rutter, E.H. (Eds.), Deformation Mechanisms, Rheology and Tectonics. The Geological Society, London, pp. 259–284.
- Wang, Y., Durham, W.B., Getting, I.C., Weidner, D.J., 2003. The deformation-DIA: A new apparatus for high temperature triaxial deformation to pressures up to 15 GPa. Rev. Sci. Instrum. 74, 3002–3011.
- Weidner, D.J., 2018. Rheological studies at high pressure. Ultrahigh Press. Mineral.  $493\mbox{-}524.$
- Zha, C.-S., Mibe, K., Bassett, W.A., Tschauner, O., Mao, H.-K., Hemley, R.J., 2008. P-V-T equation of state of platinum to 80 GPa and 1900 K from internal resistive heating/xray diffraction measurements. J. Appl. Phys. 103, 054908.
- Zhang, Z., Karato, S.I., 2021. The effect of pressure on grain-growth kinetics in olivine aggregates with some geophysical applications. J. Geophys. Res. Solid Earth 126, e2020JB020886.
- Zou, Y., Gréaux, S., Irifune, T., Whitaker, M.L., Shinmei, T., Higo, Y., 2012. Thermal equation of state of Mg 3 Al 2 Si 3 O 12 pyrope garnet up to 19 GPa and 1,700 K. Phys. Chem. Miner. 39, 589–598.